Journal of Inorganic Biochemistry 257 (2024) 112612

Contents lists available at ScienceDirect

Journal of Inorganic Biochemistry

journal homepage: www.elsevier.com/locate/jinorgbio

Design and anticancer behaviour of cationic/neutral half-sandwich iridium (III) imidazole-phenanthroline/phenanthrene complexes

Ao Lv [a], Guangxiao Li [a], Pei Zhang [b], Rui Tao [a], Xiaoshuang Li [a], Xueyan Ren [a], Peixuan Li [a], Xicheng Liu [a,*], Xiang-Ai Yuan [a], Zhe Liu [a,*]

[a] Key Laboratory of Life-Organic Analysis of Shandong Province, Institute of Anticancer Agents Development and Theranostic Application, School of Chemistry and Chemical Engineering, Qufu Normal University, Qufu 273165, Shandong, China
[b] College of Life Sciences, Qufu Normal University, Qufu 273165, Shandong, China

ARTICLE INFO

Keywords:
Iridium(III) complex
Imidazole-phenanthroline
Imidazole-phenanthrene
Anticancer
Apoptosis
Lysosomal targeted

ABSTRACT

Considerable attention has been devoted to the exploration of organometallic iridium(III) (Ir^{III}) complexes for their potential as metallic anticancer drugs. In this study, twelve half-sandwich Ir^{III} imidazole-phenanthroline/phenanthrene complexes were prepared and characterized. Complexes exhibited promising *in-vitro* antiproliferative activity, and some are obviously superior to cisplatin towards A549 cells. These complexes possessed suitable fluorescence, and a non-energy-dependent uptake pathway was identified, subsequently leading to their accumulation in the lysosome and the lysosomal damage. Additionally, complexes could inhibit the cell cycle (G1-phase) and catalyze intracellular NADH oxidation, thus substantiating the elevation of intracellular reactive oxygen species (ROS) level, which confirming the oxidative mechanism. Western blotting further confirmed that complexes could induce A549 cell apoptosis through the lysosomal-mitochondrial anticancer pathway, which was inconsistent with cisplatin. In summary, these complexes offer fresh concepts for the development of organometallic non-platinum anticancer drugs.

1. Introduction

Today, cancer is one of the most important diseases endangering human life and health. Cisplatin, a clinically utilized metal-based anticancer drug, offers a fresh concept for the creation of metallic anticancer medications [1,2]. While widely used in clinic, platinum-based drugs exhibit the disadvantages of drug resistance, serious toxicity (including renal toxicity, gastrointestinal toxicity, ototoxicity and neurotoxicity) and low biological selectivity, which limiting the long cycle and large dose use in clinical practice [3,4]. Therefore, non-platinum anticancer agents, which showing different mechanism from cisplatin, including iridium(III) (Ir^{III}) anticancer complexes, have received extensive attention as the substitutes for platinum drugs [5–7].

Ir^{III} anticancer complexes are typically classified into two distinct structural categories: Half-sandwich and cyclometallic Ir^{III} complexes [8]. Compared to cyclometallic complexes, half-sandwich Ir^{III} complexes exhibited superior anticancer activity, and their fluorescence properties could also be improved by regulating the peripheral ligands, which providing the convenient condition for the ascertainment of their anticancer mechanism [9]. In contrast to platinum-based drugs, half-sandwich Ir^{III} complexes have been reported to predominantly accumulate in intracellular mitochondria or lysosomes, which facilitating their active participation in intracellular REDOX reactions, then promoting the buildup of intracellular ROS and the induction of cell apoptosis [10]. Half-sandwich Ir^{III} complexes are commonly described as $[(\eta^5\text{-}Cp^X)Ir(L)(Z)_2]^{n+}$ or $[(\eta^5\text{-}Cp^X)Ir(L\hat{}L)Z]^{n+}$, and the screening of peripheral ligands (Cp^X (cyclopentadiene derivatives), L/L^L (monodentate or bidentate ligand), or Z (leaving group, usually chlorine)) can effectively regulate the anticancer activity of these complexes [7,11–16]. Now, the activity regulation is mainly focusing on the

Abbreviations: Cp*, pentamethyl cyclopentadiene; Cp^{xph}, phenyltetramethyl cyclopentadiene; MTT, (3-(4,5-dimethylmercaptan-2-yl)-2,5-diphenylmethyl bromide); IC_{50}, 50% inhibiting concentration; HOMO, the highest occupied molecular orbital; LUMO, the lowest unoccupied molecular orbital; CCCP, carbonyl cyanide *m*-chlorophenyl hydrazine; LTDR, lysotracker deep red, lysosome probe; MTDR, mitotracker deep red, mitochondrial probe; PCC, Pearson co-localization coefficient; PI, propidium iodide; ROS, reactive oxygen species; MMP, mitochondrial membrane potential; JC-1, (5,5′,6,6′-tetrachloro-1,1′,3,3′-tetraethylbenzimidazolyl iodocarbocyanine); NADH, nicotinamide adenine dinucleotide; TON, turnover number; WCR, wound closure rate.

* Corresponding authors.
E-mail addresses: chemlxc@163.com (X. Liu), liuzheqd@163.com (Z. Liu).

https://doi.org/10.1016/j.jinorgbio.2024.112612
Received 16 February 2024; Received in revised form 17 April 2024; Accepted 13 May 2024
Available online 15 May 2024

screening of monodentate/bidentate ligands, especially for bidentate ligands, including N^N (*e.g.*, bipyridine, phenanthroline), N^C (*e.g.*, phenylpyridine, *β*-carboline [17]), N^O (*e.g.*, acylhydrazone, picolinic acid, amino acid), N^S (*e.g.*, thiocarbazone, 2-pyridinecarbothioamide [18]), O^O (*e.g.*, *β*-diketonato [19]), *etc.*, which showing the better activity. Among them, the most studied were N^N and N^C ligands. Sadler reported series of organoiridium bipyridine (N^N)/phenylpyridine (N^C) complexes for the first time, which showed the greater potency than cisplatin in targeting a variety of cancer cells, including colon cancer, leukemia, prostate cancer, breast cancer, and melanoma [20].

The composition of many natural and semi-synthetic opioids including morphine, codeine, and naloxone, consisting of planar aromatic molecules, is commonly occurring in nature. Over the past two decades, imidazo-phenanthroline/phenanthrene or derivatives had garnered escalating interest in the fields of molecular switches, photocatalyses, luminescent sensing, photodynamic therapy (PDT), and anticancer drugs, which contributing to their strong binding with transition metals, *p*-delocalized molecular skeleton, pH dependence and structural controllability for substituents (imidazole ring) to easily adjust their optical and bioactivity characteristics [21–25]. Therefore, imidazo-phenanthroline/phenanthrene derivatives were extensively used in the synthesis of various transition metallic anticancer complexes, including Ir^{III} [26], Ru^{II} [27], Zn^{II} [28], and Rh^{I} [29]. Among them, the investigation of Ir^{III}-based complexes has harvested significant attention due to their good photophysical properties, exceptional chemical stability, and promising anticancer activity. Long-term lysosome tracking was achieved *via* endocytic trafficking of a self-assembling Ir^{III} imidazo-phenanthroline complex, as demonstrated by Chao et al. [23] Guo et al. prepared two benzothiophenyliso-quinoline-derived Ir^{III} complexes, which showed the first instance of ferroptosis caused by photosensitive Ir^{III} complexes [30]. Chao et al. obtained a mitochondrial-targeting Ir^{III} imidazo-phenanthroline prodrug, which was responsive to the tumor microenvironment and able to release two-photon photosensitizers for PDT and a glutathione scavenger [22]. Of course, these reports were primarily on cyclometallic Ir^{III} complexes, with less emphasis on half-sandwich Ir^{III} complexes.

In this study, six imidazo-phenanthroline/phenanthrene pro-ligands were prepared, then reacted with basic Ir^{III} precursors and obtained twelve ionic/neutral half-sandwich Ir^{III} imidazole complexes (**Ir1-Ir12**, Chart 1) in this study. The potential of these complexes inhibiting cancer cell proliferation was initially evaluated *in vitro* using the MTT (3-(4,5-Dimethylthiazol-2-yl)-2,5-diphenyltetrazolium bromide) assay. Additionally, the representative complex (**Ir6**) was selected as a model to evaluate anti-migration, intracellular imaging, anticancer mechanism, and anticancer channel of these complexes [31].

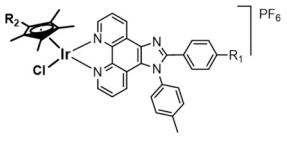

Ir1–Ir6

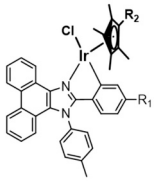

Ir7–Ir12

Complexes	R_1	R_2
Ir1	F	CH_3
Ir2	F	C_6H_5
Ir3	H	CH_3
Ir4	H	C_6H_5
Ir5	OCH_3	CH_3
Ir6	OCH_3	C_6H_5
Ir7	F	CH_3
Ir8	F	C_6H_5
Ir9	H	CH_3
Ir10	H	C_6H_5
Ir11	OCH_3	CH_3
Ir12	OCH_3	C_6H_5

Chart 1. Structures of half-sandwich iridium(III) imidazole-phenanthroline/phenanthrene complexes.

2. Results and discussion

2.1. Synthesis and structural characterization

The imidazole-based pro-ligands (L1-L6) were synthesized using a usual four components assembling of 1,10-phenolin-5,6-dione/acenaphthenedione, ammonium acetate, 4-methylaniline and the corresponding benzaldehyde (-F/-H/-OCH_3; Scheme 1), and the pure products were achieved through column chromatography (petroleum ether: ethyl acetate = 15:1). Target complexes were prepared through the reaction of basic Ir^{III} precursors ($([(\eta^5\text{-Cp}^*)Ir(\mu\text{-Cl})Cl]_2$, Dimer 1; $[(\eta^5\text{-Cp}^{xph})Ir(\mu\text{-Cl})Cl]_2$, Dimer 2) and twice the proportion of imidazole chelating ligands. Phenanthrene-based complexes (**Ir7-Ir12**, $[(\eta^5\text{-Cp}^X)Ir(C^N)Cl]$) were obtained by adding sodium acetate as an acid binding agent, and phenanthroline-based one were precipitated into hexafluorophosphate (**Ir1-Ir6**, $[(\eta^5\text{-Cp}^X)Ir(N^N)Cl]PF_6$). Characterization was carried out using NMR and MS spectra. In the cyclopentadiene ($\eta^5\text{-Cp}^X$) ligand, the hydrogen atoms of methyl were observed in the range of 1.5–2.0 ppm, and those on the planar imidazo-phenanthroline/phenanthrene were in the range of 7.5–9.5 ppm [32,33]. The results of MS were consistent with the theoretical calculations ($[M\text{-}PF_6]^+$ for **Ir1-Ir6**; $[M\text{-}Cl]^+$ for **Ir7-Ir12**).

Typically, the anticancer activity of half-sandwich Ir^{III} complexes is typically attributed to hydrolysis (the broken of Ir—Cl bond), and Ir-H_2O exhibiting the higher activity in comparison to the corresponding halides [34]. Hydrolysis is a major step to exert activity for these complexes. The hydrolysis characteristics of these complexes were determined in a solution of DMSO 20%/H_2O 80% (*v*/*v*) using ultraviolet-visible (UV–Vis) spectroscopy over a duration of 8 h, **Fig. S5**. However, these complexes exhibit the different properties from the classical half-sandwich Ir^{III} complexes, which are relatively stable and do not undergo hydrolysis. Furthermore, the stability of **Ir2** in solution was identified through the ^1H NMR spectra, **Fig. S6**. As shown, in both the pure DMSO solvent and the mixed 80% DMSO-d_6/20% D_2O (*v*/*v*) solution, **Ir2** still exhibits good stability after 24 h of incubation. This conclusion implies that these complexes possess a distinct anticancer mechanism in comparison to the traditional Ir^{III} complex, and this stability also provides a convenient condition for the further investigation of biological properties.

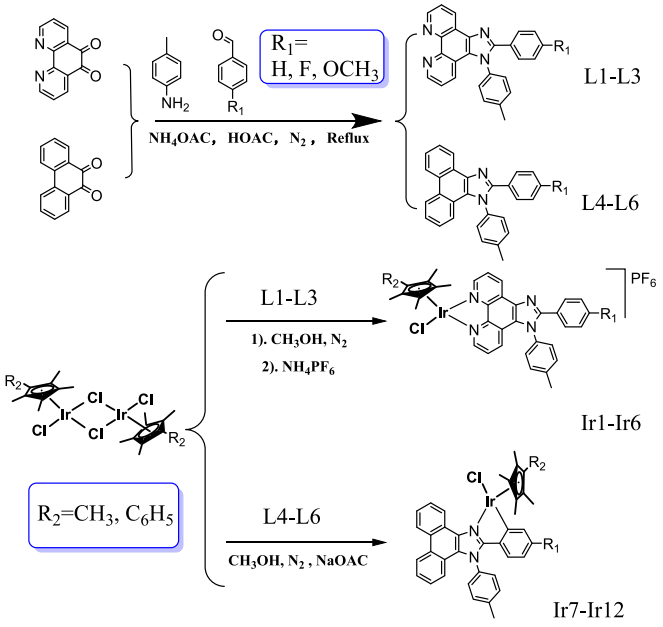

Scheme 1. Design of imidazole proligands (**L1-L6**) and target complexes (**Ir1-Ir12**).

2.2. In-vitro proliferation and migration inhibition

A549 cell line (lung epithelial carcinoma, the most common cancer of in the developed and developing regions) was incubated with these complexes for a duration of 24 h and estimated through MTT assay in this study [35]. Cisplatin, commonly utilized in clinical settings, was employed as a reference to distinguish their *in-vitro* anti-proliferative activity, and the IC_{50} values (the concentration at which there is a 50% inhibition of cell growth, a crucial parameter for assessing bioactivity) were listed in Table 1. These complexes exhibit promising anti-proliferative activity, especially for the η^5-Cp^{xph}-based one, all of which possess superior activity to cisplatin under the same conditions. However, the substituents on imidazole ligands (F/H/OCH_3, which represent the different absorption and electron donor properties) exhibit the weaker effect on the activity, including variations in coordination modes of imidazole ligands (N^N or C^N). Among these complexes, **Ir6**, L3-based complex exhibits the superior activity, which is even twice as good as cisplatin. Even after 72 h of treatment, **Ir6** continues to perform well, including the A549/DDP (cisplatin-resistance) cells, **Table S1**. However, **Ir6** shows the worse potential for other cancer cells, including HepG2, Hela, HT29 and HCT116 cell lines, **Table S2**. Cytotoxic effect on BEAS-2B cells (human normal bronchial epithelial cells) were also determined. The selectivity index (SI) for **Ir6** is 3.00, calculated as the ratio of the IC_{50} value of BEAS-2B cells to that of A549 cells, however, that for cisplatin is 1.80. This result indicates that **Ir6** has less cytotoxicity and better anti-proliferative activity than cisplatin under the same conditions, then possessing favorable anticancer potency.

The bioactivity of organometallic complexes hinges upon a crucial indicator: Energy gap between the highest occupied molecular orbital (HOMO) and the lowest unoccupied molecular orbital (LUMO). Organometallic complex generally shows a better reactivity when the HOMO and LUMO orbital energy range is smaller [36–38]. Then, the orbital energy ranges of **Ir5, Ir6, Ir11**, and **Ir12** were determined through a calculation through density functional theory (DFT) using the DFT/B3LYP-D3/6-31G(d, p)(C, H, N, Cl)/LANL2DZ (Ir) level in this study [39]. As shown in Fig. 1, the HOMO orbital electron cloud is mainly distributed on the central iridium ion and imidazole ligand, however, that for LUMO is mainly on Ir ion and Cp ligand. η^5-Cp^{xph}-based complexes (**Ir6**/**Ir12**) show the lower orbital energy level difference than that of the corresponding η^5-Cp*-based one (**Ir5**/**Ir11**). This finding aligns with the observed trend of *in-vitro* anti-proliferative activity. (Table 1).

The process of cancer cell metastasis involves the release of cancer cells from the primary cancerous sites and their subsequent migration to remote tissues through the lymphatic or circulatory system, resulting in the development of secondary tumor lesions [40]. Inhibiting tumor metastasis is an essential component of advanced tumor treatment [41–43]. Therefore, wound healing assay was employed to preliminarily

Table 1
IC_{50} values and selectivity index of **Ir1-Ir12** and cisplatin towards A549 and BEAS-2B cells after incubation of 24 h.

Complexes	IC_{50} (μM)		SI (BEAS-2B/A549)
	A549 cell	BEAS-2B cell	
Ir1	>100	>100	/
Ir2	18.15 ± 0.44	38.02 ± 0.33	2.09
Ir3	58.05 ± 0.40	71.99 ± 0.31	1.24
Ir4	15.73 ± 0.29	27.11 ± 0.69	0.13
Ir5	>100	97.16 ± 0.42	/
Ir6	11.49 ± 0.27	34.52 ± 0.18	3.00
Ir7	22.93 ± 0.34	19.19 ± 0.23	0.84
Ir8	15.15 ± 0.62	26.03 ± 0.58	1.71
Ir9	66.37 ± 0.16	70.22 ± 0.36	1.05
Ir10	15.54 ± 0.31	24.33 ± 0.24	1.57
Ir11	97.41 ± 0.14	>100	/
Ir12	19.34 ± 0.52	28.02 ± 0.32	1.45
Cisplatin	21.32 ± 1.71	38.43 ± 0.62	1.80

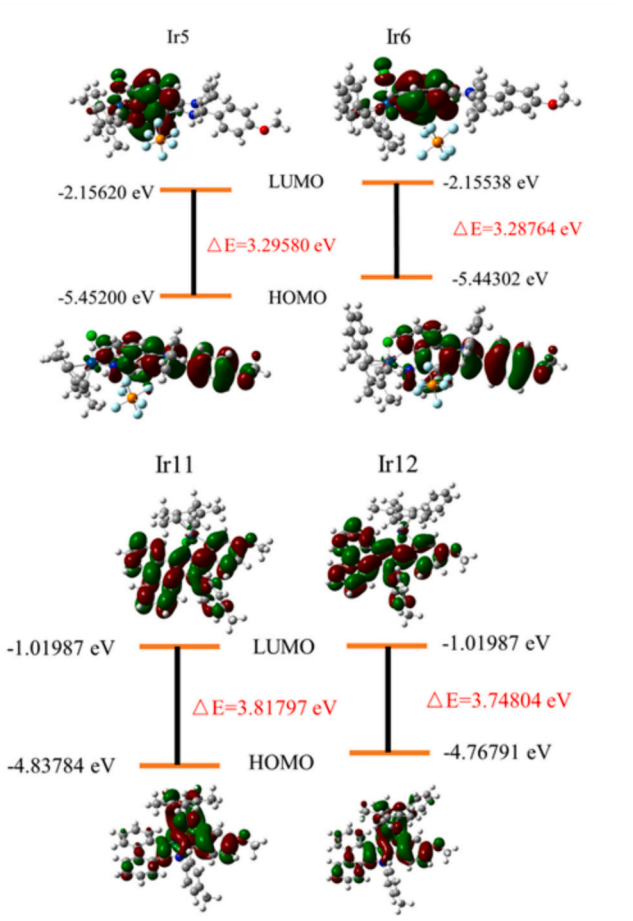

Fig. 1. Electron cloud distribution of frontier orbitals (HOMO and LUMO) and the energy levels of **Ir5, Ir6, Ir11** and **Ir12**.

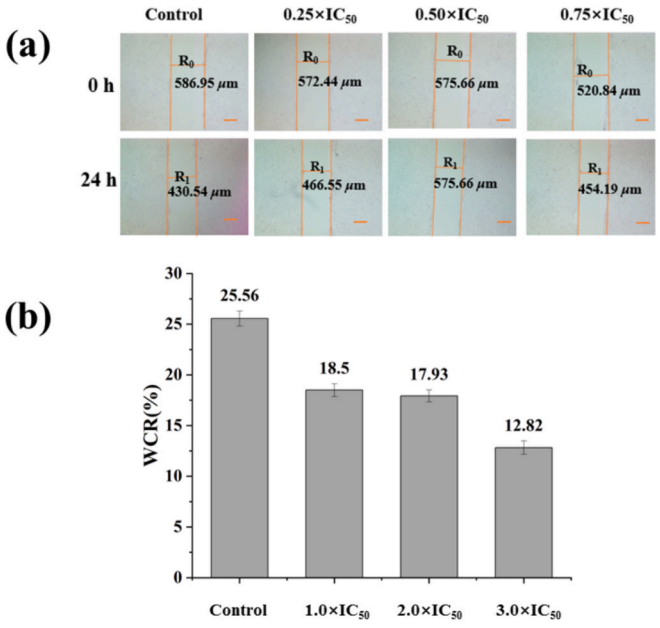

Fig. 2. (a) Photographs of wound healing against A549 cells following the treatment of **Ir6**. Scale bar: 200 μM; **(b)** Bar chart of WCR values after the treatment of **Ir6**.

evaluate the anti-metastasis potential of these complexes towards A549 cells in this study. As Fig. 2 demonstrated, R_0 and R_1 represent the breadth of "wounds" (the areas free of A549 cells) after the treatment of **Ir6** (specially selected complex, which demonstrating the best activity among these complexes) for 0 h and 24 h. The values of wound closure rate (WCR), calculated by WCR = $(R_0\text{-}R_1)/R_0 \times 100\%$, exhibit a dose-dependent reduction after the treatment of **Ir6**. The value of WCR is only half that of the control after the incubation of **Ir6** at 0.75 × IC_{50}. Above all, including promising anti-proliferative properties, **Ir6** also possesses the anti-migratory capability. Therefore, **Ir6** is selected as a representative to investigate the underlying anticancer mechanism of these complexes.

2.3. Cellular localization analysis

Drugs with good intracellular absorption routes are able to enter cells easily and show physiological effects. For organometallic complexes, energy-dependent mode (*e.g.*, active transport and endocytosis) and non-energy-dependent mode (*e.g.*, passive transport and free diffusion) are two main cellular uptake mechanism [44,45]. **Ir6** shows a strong absorption at 320 nm and a weak absorption observed at 410 nm attributing to the π-π* transition and the metal-ligand charge transfer transition, respectively, then accompanied by an emission at 486 nm (**Fig. S7**). Therefore, A549 cells were pretreated with chloroquine (endocytosis modulator) or carbonyl cyanid-*m*-chlorophenylhydrazone (CCCP, metabolism inhibitor) for 2 h, then subsequently incubated with **Ir6** at 310 K/277 K to investigate the uptake mode, Fig. 3a. As shown, the smooth entry into A549 cells under all conditions confirms that **Ir6** follows a non-energy-dependent cellular uptake mode.

As shown in Fig. 3b, using the laser confocal microscopy, the intracellular co-localization of **Ir6** was detected based on its suitable emission without any interference with MitoTracker Deep Red (MTDR) and LysoTracker Deep Red (LTDR), the conventional mitochondrial and lysosomal probe, respectively [46]. Evidently, **Ir6** could accumulate in the intracellular lysosomes of A549 cells following a Pearson co-localization coefficient (PCC) of 0.70, however, that is only 0.20 for mitochondria, which indicating that lysosomes are the main target locations in A549 cells. Interestingly, the presence of **Ir6** does not induce A549 cell death immediately, which opens up the possibility of studying the changes of lysosome morphology timely. Once lysosome injury, the subsequent release of enzymes into the cytoplasm can trigger cell apoptosis or necrosis [47–50]. Typically, lysosome integrity can be determined through acridine orange (AO, an acid fluorescent probe), which demonstrates red fluorescence emission within the lysosome and green fluorescence emission within the cytoplasm. Therefore, A549 cells were treated with **Ir6** (1.0 × IC_{50}) over times, then stained with AO to assess the lysosomal integrity. As shown in Fig. 3c, in the control group, a significant amount of red fluorescence is observed, indicating the intact lysosomes. However, after the treatment of **Ir6**, the loss of red emission becomes readily discernible with the naked eyes, which indicating the damage of lysosomal integrity and subsequent cell death of A549 cells.

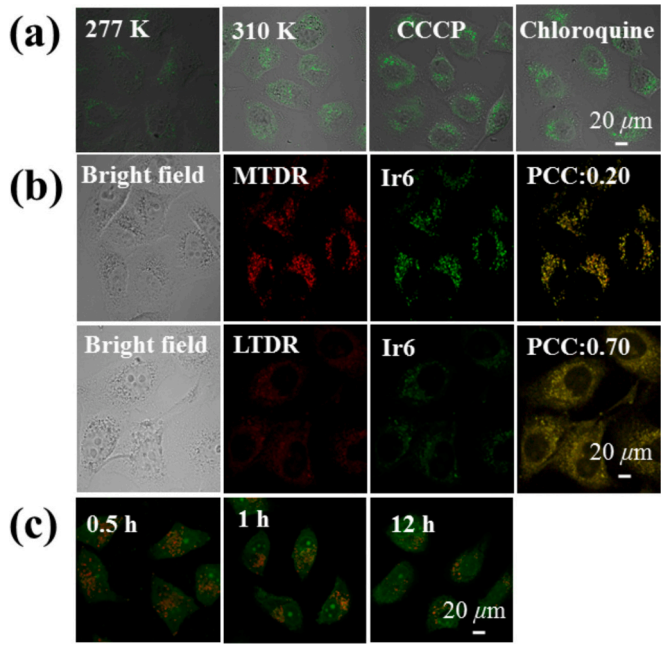

Fig. 3. (a) Photomicrographs of A549 cells after treated with CCCP/chloroquine and **Ir6**; **(b)** Photomicrographs of A549 cells after incubation of MTDR/LTDR and **Ir6**. **Ir6**, MTDR and LTDR was excited at 405, 644 and 594 nm, then collected at 500 ± 70, 690 ± 30 and 630 ± 30 nm, respectively; **(c)** Photomicrographs of A549 cells after the incubation of **Ir6** and AO. Scale bar: 20 μm.

2.4. Apoptosis assay

Cell apoptosis is a highly regulated process in which cells undergo programmed cell death to maintain tissue homeostasis, and this process is regulated and accompanied by distinct cell morphological alterations [51]. Metallic complexes typically exert their anticancer effects through the induction of apoptosis [52]. Then the effect of **Ir6** on A549 cell apoptosis was detected by a dual probe of membranin V-FITC/ Propyl iodide (PI) after the treatment for 24 h. As shown in Fig. 4a and **Table S3**, **Ir6** can significantly promote A549 cell apoptosis in a concentration-dependent mode. When **Ir6** increasing from 1.0 × IC_{50} to 3.0 × IC_{50}, there is a 22.8% increase in the proportion of apoptotic cells (including early and late apoptosis), however, the rate of survival is 87.5% in the control group. Compared with the control, the early apoptosis proportion showed a 46.45% increase, which confirming the anticancer activity of **Ir6** by inducing early apoptosis.

The essential characteristic for tumor is that cell cycle regulation is out of control and cell proliferation is infinite [53,54]. Therefore, it makes sense to develop anticancer drugs that concentrating on the inhibition of cell cycle progression. Cell cycle, *e.g.*, G1 phase (cells experience growth and prepare for DNA replication), S phase (DNA synthesis occurs) and G2 phase (cells prepare for division), refers to one cell division to the next, ultimately leading to the formation of daughter cells [55,56]. When the cell cycle is disrupted or inhibited, it can elicit various cellular responses, including apoptosis [51]. As shown in Fig. 4b and **Table S4**, the proportion of A549 cells is mainly concentrated in G1 phase, which increases by 11.63% after the incubation of **Ir6** from 0.5 × IC_{50} to 2.0 × IC_{50}, then showing a dose-dependent increase. This disruption of cell cycle is a potential mechanism through which **Ir6** exerting its effects on A549 cells.

Reactive oxygen species (ROS) are generated as inherent byproducts during cellular metabolism, particularly through aerobic respiration in the mitochondria. If excessively elevated, they can induce oxidative stress and inflict damage on various cellular components, including membrane proteins. High levels of intracellular ROS can initiate a cascade of events, including disrupting cell signaling pathways and inducing apoptosis [57,58]. In this study, the intracellular ROS levels were assessed after the treatment of **Ir6** for 24 h. To detect ROS levels, a fluorescent probe called DCFH-DA (2,7-dichlorodihydrofluorescein diacetate) was used, which would be oxidized by ROS and result is the formation of the fluorescent DCF (2,7-dichlorofluorescein), Fig. 5a. ROS levels of the experimental group are significantly improved compared to those in the control, although the increase is not significant with the increase of **Ir6**. A significant 2.62-fold increase is found for the intracellular ROS level after the treatment of **Ir6** at 2.0 × IC_{50} in comparison to the control.

Mitochondria could convert cellular energy and serve as reservoirs for storing electrochemical potential energy within cell membranes. An uneven distribution of protons or other ions across the inner membrane

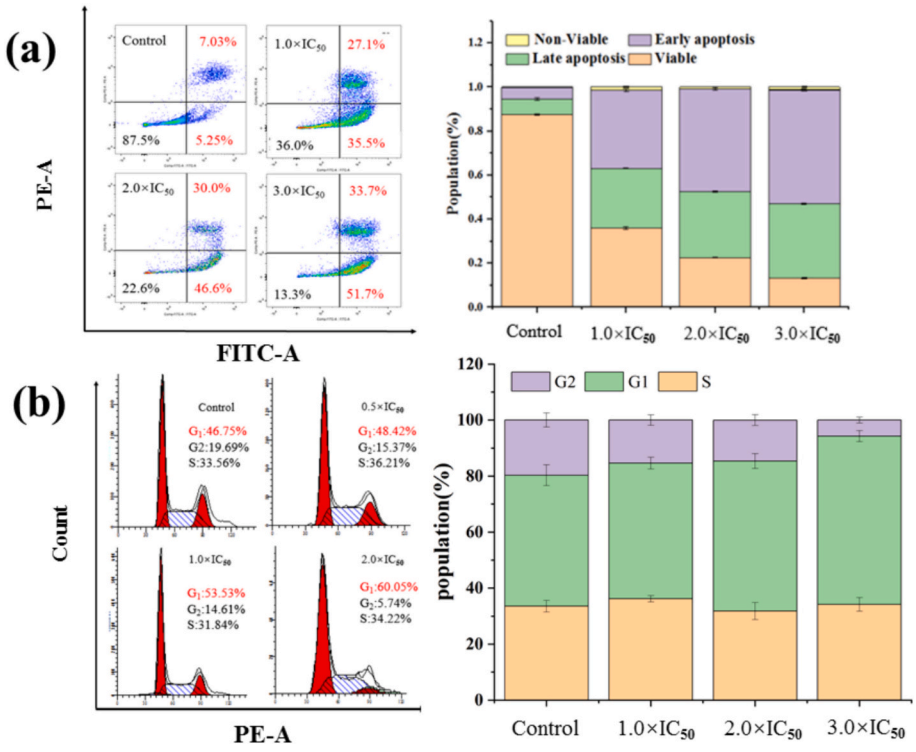

Fig. 4. **(a)** Statistical analysis and histograms of apoptotic A549 cells after treated with **Ir6** and dyed with Annexin VFITC/PI; **(b)** Cell cycle distribution ratio and histograms of A549 cells after treated with **Ir6** and dyed with PI/RNase. Data were quoted as mean ± SD of three replicates.

could lead to the decline of mitochondrial membrane potential (MMP), then accompanied by an improvement of intracellular ROS level [59]. Hence, to investigate the state of MMP, A549 cells were exposed to **Ir6** and subsequently labeled with JC-1 (an efficient fluorescent probe, which emitting red or green fluorescence depending on its existence in monomeric or aggregated forms, then corresponding to an increase or decrease of intracellular MMP, respectively), Fig. 5b and **Table S5**. As shown, the proportion of mitochondrial membrane depolarized cells (highlighted by green fluorescence) increases by 70.41% with the increase of **Ir6** (0.5 × IC_{50} to 3.0 × IC_{50}), then showing a dose-dependent improvement. Furthermore, NADH, the reduced form of nicotinamide adenine dinucleotide, is essential as a regulatory marker for the energy production process within mitochondria. Assessing the redox state of NADH serves as a valuable parameter for characterizing the mitochondrial activity *in vivo* [60]. Typically, organometallic complexes could usually accelerate the oxidation of NADH, then inducing the improvement of intracellular ROS levels [61]. Therefore, NADH was hatched with **Ir6** in a solution of 20% CH_3OH and 80% H_2O (*v*/*v*), then monitored by UV–Vis spectra to detect the time-dependent interaction between them. As shown in Fig. 5c, the absorbance at 259 nm (NAD^+, the oxidation state of NADH after losing hydrogen) and 339 nm (NADH) increases and decreases after the incubation. These changes are conveniently detected through a turnover number (TON, 60.1), which further ascertaining the favorable biocatalysis property of **Ir6**. Above all, despite of primarily accumulating in lysosomes without significant mitochondrial targeting, **Ir6** can cause the lysosomal damage, resulting in the hydrolases entering the cytoplasm, then acting on mitochondria and reducing MMP, increasing the intracellular ROS level, and presenting a lysosomal-mitochondria apoptotic channel.

To further understand the effect of lysosomes and mitochondria on **Ir6**-induced apoptosis, the expression levels of lysosomal membrane protein (LAMP-1), cytochrome C oxidase (Cyt—C), and cathepsin (CB) were determined using Western blotting, Fig. 6 [62,63]. As shown, the expression of LAMP-1 significantly downregulates, indicating a decrease in lysosomal integrity. On the other hand, the expression levels of CB and Cyt-C upregulate. Based on these results, it can be inferred that **Ir6** can interact with LAMP-1 protein, leading to extensive lysosomal membrane permeability, releasing cathepsin CB into the cytoplasm originally presenting in lysosomes, inducing the change of MMP, then finally releasing pro-apoptotic factor Cyt-C and leading to apoptosis. The results obtained from the downregulation of LAMP-1 and upregulation of CB and Cyt-C strongly support the hypothesis that **Ir6** follows a lysosomal-mitochondrial apoptotic pathway.

3. Conclusion

In this study, a total of twelve cationic/neutral half-sandwich Ir^{III} imidazole complexes were synthesized and characterized. These complexes showed favorable stability in the biological test environment, exhibiting distinct characteristics compared to the traditional half-sandwich Ir^{III} complexes. Complexes had good anti-proliferative and anti-migration ability towards A549 cancer cells, especially for η^5-Cp^{xph}-based one. **Ir6**, L3-based complex, possessed the best activity among these complexes, which was even twice as good as cisplatin against A549 cells. Meanwhile, Ir6 showed the better activity towards A549/DDP cells and the less cytotoxicity, then being a potential substitute for cisplatin. **Ir6** entered into A549 cells through a non-energy-dependent mode, specifically targeting intracellular lysosomes and causing the disruption of lysosomal integrity. Moreover, **Ir6** exhibited the ability of accelerating NADH oxidation, leading to a reduction in MMP and improvement of intracellular ROS levels, disrupting the cell cycle at the G1 phase, and ultimately inducing apoptosis. Western blotting further confirmed **Ir6** following a lysosomal-mitochondrial anticancer pathway and showing a different anticancer mechanism from cisplatin. However, most of the objective complexes are highly toxic in comparison to cisplatin and show the worse activity towards cancer cells other than A549 cells. Additionally, the modification of peripheral ligands shows little effect on the activity, which also requiring further adjustment to improve. Above all, half-sandwich Ir^{III} imidazole complex may be a potential substitute for platinum-based drugs and warrant further study.

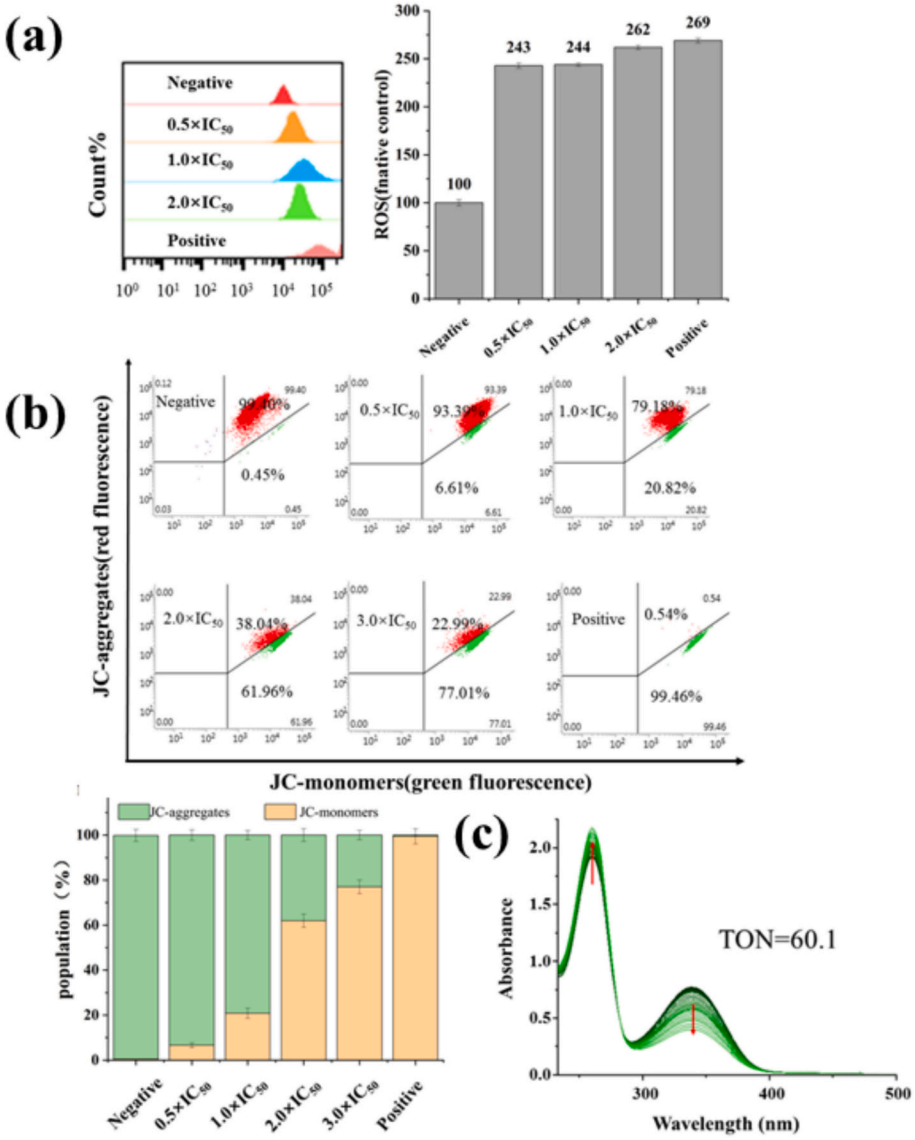

Fig. 5. **(a)** Intracellular ROS levels after the treatment of **Ir6** for 24 h; (b) The proportion of JC-1 aggregates and JC-1 monomers because of **Ir6**; (c) UV–Vis spectra of NADH (100 μM) in 20% MeOH/80% H_2O (v/v) inducing by Ir6 (1.0 μM) over 8 h.

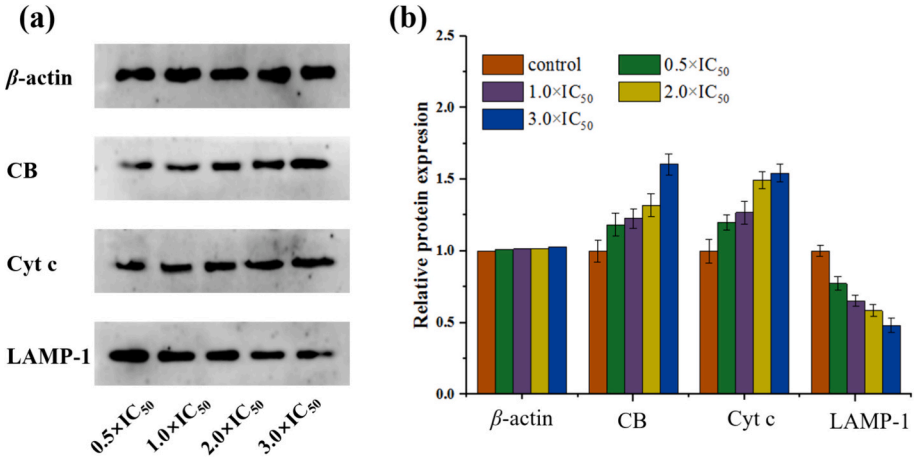

Fig. 6. **(a)** Protein expression (LAMP-1, CB, and Cyt C) after the treatment of **Ir6** at a gradient concentration. To ensure equal protein loading, β-Actin was used as a loading control; **(b)** Histograms depicted the alterations in protein expression across a range of concentrations.

4. Experimental section

4.1. General information

All synthesized materials and organic solvents were purchased from Rhea Biotechnology Co. LTD and used without further treatment. The fundamental iridium precursors ($[(\eta^5\text{-Cp}^*)\text{Ir}(\mu\text{-Cl})\text{Cl}]_2$, Dimer 1; $[(\eta^5\text{-Cp}^{xph})\text{Ir}(\mu\text{-Cl})\text{Cl}]_2$, Dimer 2) were prepared following the literature procedures [20]. Imidazole-phenanthroline/ phenanthrene pro-ligands (L1-L6) were prepared according to the reported methods [64,65].

4.2. Synthesis of half-sandwich Ir^{III} imidazole complexes (Ir1-Ir6)

Under a nitrogen atmosphere, a mixture of basic iridium precursors (Dimer1/2, 0.10 mmol) and twice the proportion of the imidazole-phenanthroline ligands (L1-L3, 0.20 mmol) was dissolved in methanol (30 mL) and stirred at room temperature for 24 h. Then, ammonium hexafluorophosphate (0.80 mmol) was added and reacted for another 6 h. The solvent was removed under vacuum, and 3 mL dichloromethane was added. After filtration, yellow products (**Ir1-Ir6**) were obtained by adding *n*-hexane (30 mL) to facilitate diffusion. The NMR and MS spectra were depicted in **Figs. S3-S4** The data were as follows:

Ir1: Yield 101.8 mg (55.8%). ^{1}H NMR (500 MHz, DMSO) δ 9.37 (dd, J = 8.1, 7.0 Hz, 2H), 9.26 (d, J = 5.2 Hz, 1H), 8.31 (dd, J = 8.2, 5.3 Hz, 1H), 7.99 (dd, J = 8.6, 5.3 Hz, 1H), 7.73–7.66 (m, 3H), 7.64 (dd, J = 8.4, 5.1 Hz, 2H), 7.57 (d, J = 8.3 Hz, 2H), 7.30 (t, J = 8.9 Hz, 2H), 2.52 (d, J = 6.4 Hz, 3H, CH_3), 1.51 (s, 15H, Cp-CH_3). ESI-MS (m/z): Calcd for $C_{36}H_{32}N_4ClF_7PIr$, 912.1571; Found 767.1982, $[M\text{-}PF_6]^+$. Elem. anal. Calcd for $C_{36}H_{32}N_4F_7PClIr$: C, 47.40; H, 3.54; N, 6.14%; Found C, 47.63; H, 3.61; N, 6.02%.

Ir2: Yield 105.8 mg (54.3%). ^{1}H NMR (500 MHz, $CDCl_3$) δ 9.24 (d, J = 8.2 Hz, 1H), 8.84 (d, J = 5.1 Hz, 1H), 8.70 (d, J = 5.3 Hz, 1H), 7.84 (dd, J = 8.2, 5.4 Hz, 1H), 7.67 (dd, J = 8.6, 5.2 Hz, 1H), 7.61 (dd, J = 7.3, 4.1 Hz, 3H), 7.55 (dd, J = 8.7, 5.3 Hz, 2H), 7.51–7.46 (m, 5H), 7.38 (d, J = 7.6 Hz, 1H), 7.25 (d, J = 8.6 Hz, 1H), 6.97 (t, J = 8.6 Hz, 2H), 2.51 (s, 3H, CH_3), 1.82 (s, 3H, Cp-CH_3), 1.76 (d, J = 6.4 Hz, 6H, Cp-CH_3), 1.66 (s, 3H, Cp-CH_3). ESI-MS (m/z): Calcd for $C_{41}H_{34}N_4ClF_7PIr$, 974.1727; Found 829.2066, $[M\text{-}PF_6]^+$. Elem. anal. Calcd for $C_{41}H_{34}N_4F_7PClIr$: C, 50.54; H, 3.52; N, 5.75%; Found C, 50.62; H, 3.59; N, 7.66%.

Ir3: Yield 91.6 mg (51.2%). ^{1}H NMR (500 MHz, $CDCl_3$) δ 9.27 (d, J = 8.0 Hz, 1H), 9.10 (d, J = 8.0 Hz, 1H), 8.02 (t, J = 7.5 Hz, 1H), 7.54 (d, J = 7.7 Hz, 2H), 7.47 (d, J = 8.0 Hz, 2H), 7.34 (t, J = 7.6 Hz, 2H), 7.20 (dd, J = 13.6, 5.9 Hz, 4H), 6.85–6.80 (m, 2H), 2.48 (s, 3H, CH_3), 1.60 (s, 15H, Cp-CH_3). ESI-MS (m/z): Calcd for $C_{36}H_{33}N_4ClF_6PIr$, 894.1665; Found 749.2047, $[M\text{-}PF_6]^+$. Elem. anal. Calcd for $C_{36}H_{33}N_4F_6PClIr$: C, 48.35; H, 3.72; N, 6.26%; Found C, 48.66; H, 3.81; N, 6.18%.

Ir4: Yield 102.5 mg (53.6%). ^{1}H NMR (500 MHz, DMSO) δ 9.36 (d, J = 8.2 Hz, 1H), 9.08 (d, J = 6.2 Hz, 1H), 8.97 (d, J = 5.2 Hz, 1H), 8.25 (dd, J = 8.2, 5.3 Hz, 1H), 7.94 (dd, J = 8.6, 5.3 Hz, 1H), 7.73 (dd, J = 8.1, 2.3 Hz, 1H), 7.63 (dd, J = 11.0, 5.5 Hz, 5H), 7.54 (dd, J = 14.2, 7.7 Hz, 5H), 7.50 (d, J = 6.3 Hz, 2H), 2.50 (d, J = 2.7 Hz, 3H, CH_3), 1.83 (s, 6H, Cp-CH_3), 1.73 (m, J = 2.6 Hz, 6H, Cp-CH_3). ESI-MS (m/z): Calcd for $C_{41}H_{35}N_4ClF_6PIr$, 956.1821; Found 811.2179, $[M\text{-}PF_6]^+$. Elem. anal. Calcd for $C_{41}H_{35}N_4F_6PClIr$: C, 51.49; H, 3.69; N, 5.86%; Found C, 51.75; H, 3.77; N, 5.75%.

Ir5: Yield 99.6 mg (53.9%). ^{1}H NMR (500 MHz, $CDCl_3$) δ 9.32 (d, J = 8.2 Hz, 1H), 9.10 (d, J = 5.3 Hz, 1H), 9.07 (d, J = 5.1 Hz, 1H), 8.09 (dd, J = 8.2, 5.3 Hz, 1H), 7.85 (dd, J = 8.6, 5.3 Hz, 1H), 7.65 (d, J = 8.6 Hz, 1H), 7.57 (d, J = 8.7 Hz, 2H), 7.52 (dd, J = 8.1, 6.1 Hz, 2H), 7.46 (d, J = 8.1 Hz, 1H), 7.31 (d, J = 9.9 Hz, 1H), 6.86 (d, J = 8.8 Hz, 2H), 3.82 (s, 3H, OCH_3), 2.59 (s, 3H, CH_3), 1.75 (s, 15H, Cp-CH_3). ESI-MS (m/z): Calcd for $C_{37}H_{35}N_4OF_6PClIr$, 924.1770; Found 779.2182, $[M\text{-}PF_6]^+$. Elem. anal. Calcd for $C_{37}H_{35}ON_4ClF_6PIr$: C, 48.08; H, 3.82; N, 6.06%; Found C, 48.31; H, 3.91; N, 5.96%.

Ir6: Yield 103.0 mg (52.2%). ^{1}H NMR (500 MHz, $CDCl_3$) δ 9.30 (d, J = 8.2 Hz, 1H), 8.91 (d, J = 5.1 Hz, 1H), 8.77 (d, J = 5.3 Hz, 1H), 7.93–7.89 (m, 1H), 7.76–7.72 (m, 1H), 7.66 (d, J = 7.9 Hz, 3H), 7.55 (d, J = 5.4 Hz, 4H), 7.45 (d, J = 7.7 Hz, 2H), 7.33 (d, J = 8.0 Hz, 2H), 6.85 (d, J = 8.8 Hz, 3H), 3.81 (s, 3H, OCH_3), 2.58 (s, 3H, CH_3), 1.88 (s, 3H, Cp-CH_3), 1.81 (d, J = 5.3 Hz, 6H, Cp-CH_3), 1.75 (s, 3H, Cp-CH_3). ESI-MS (m/z): Calcd for $C_{42}H_{37}ON_4ClF_6PIr$, 986.1927; Found 841.2221, $[M\text{-}PF_6]^+$. Elem. anal. Calcd for $C_{42}H_{37}N_4F_6POClIr$: C, 51.14; H, 3.78; N, 5.68%; Found C, 51.32; H, 3.83; N, 5.55%.

4.3. Synthesis of half-sandwich Ir^{III} imidazole complexes (Ir7-Ir12)

Under a nitrogen atmosphere, a mixture of basic iridium precursors (Dimer1/2, 0.10 mmol), twice the proportion of the imidazole- phenanthrene ligands (L4-L6, 0.20 mmol) and sodium acetate (0.40 mmol) was dissolved in methanol (30 mL) and refluxed for 12 h. Then, the solvent was removed under vacuum, and 3 mL dichloromethane was added. After filtration, yellow products (**Ir7-Ir12**) were obtained by adding *n*-hexane (30 mL) to facilitate diffusion. The NMR and MS spectra were depicted in **Figs. S3-S4** The data were as follows:

Ir7: Yield 85.7 mg (56.1%). ^{1}H NMR (500 MHz, $CDCl_3$) δ 9.02 (d, J = 8.9 Hz, 1H), 8.74 (t, J = 9.1 Hz, 2H), 7.91 (t, J = 7.2 Hz, 1H), 7.74 (t, J = 7.7 Hz, 1H), 7.60 (q, J = 7.2 Hz, 3H), 7.52 (d, J = 7.9 Hz, 1H), 7.47 (d, J = 7.9 Hz, 1H), 7.41 (dd, J = 8.6, 2.5 Hz, 1H), 7.33 (t, J = 7.7 Hz, 1H), 7.17 (d, J = 8.2 Hz, 1H), 6.52 (td, J = 8.6, 2.5 Hz, 1H), 6.32 (dd, J = 8.7, 5.3 Hz, 1H), 2.68 (s, 3H, CH_3), 1.60 (s, 15H, Cp-CH_3). ESI-MS (m/z): Calcd for $C_{38}H_{33}N_2ClFIr$, 764.1946; Found 729.2283, $[M\text{-}Cl]^+$. Elem. anal. Calcd for $C_{38}H_{33}N_2ClFIr$: C, 59.71; H, 4.35; N, 3.67%; Found C, 59.92; H, 4.46; N, 3.55%.

Ir8: Yield 91.2 mg (55.2%). ^{1}H NMR (500 MHz, $CDCl_3$) δ 8.76 (d, J = 7.9 Hz, 1H), 8.67 (d, J = 8.4 Hz, 1H), 8.61 (d, J = 8.2 Hz, 1H), 7.64 (t, J = 7.5 Hz, 1H), 7.58–7.53 (m, 1H), 7.49 (dd, J = 8.1, 5.7 Hz, 3H), 7.46–7.38 (m, 2H), 7.28 (q, J = 8.1 Hz, 5H), 7.19 (dd, J = 13.7, 6.6 Hz, 2H), 7.14 (d, J = 8.3 Hz, 1H), 6.90 (t, J = 8.4 Hz, 2H), 2.45 (s, 3H, CH_3), 1.83 (s, 6H, Cp-CH_3), 1.73 (m, J = 2.6 Hz, 6H, Cp-CH_3). ESI-MS (m/z): Calcd for $C_{43}H_{35}N_2ClFIr$, 826.2102; Found 791.2401, $[M\text{-}Cl]^+$. Elem. anal. Calcd for $C_{43}H_{35}N_2ClFIr$: C, 62.49; H, 4.27; N, 3.39%; Found C, 62.64; H, 4.36; N, 3.22%.

Ir9: Yield 81.8 mg (54.8%). ^{1}H NMR (500 MHz, $CDCl_3$) δ 9.26 (d, J = 8.0 Hz, 1H), 9.09 (d, J = 8.0 Hz, 1H), 8.01 (t, J = 7.5 Hz, 1H), 7.93 (t, J = 7.5 Hz, 1H), 7.53 (d, J = 7.7 Hz, 2H), 7.47 (d, J = 8.0 Hz, 2H), 7.33 (t, J = 7.6 Hz, 2H), 7.18 (dd, J = 13.6, 5.9 Hz, 4H), 6.87–6.79 (m, 2H), 2.48 (s, 3H, CH_3), 1.66 (s, 15H, Cp-CH_3). ESI-MS (m/z): Calcd for $C_{38}H_{34}N_2ClIr$, 746.2040; Found 711.2318, $[M\text{-}Cl]^+$. Elem. anal. Calcd for $C_{38}H_{34}N_2ClIr$: C, 61.15; H, 4.59; N, 3.75%; Found C, 61.44; H, 4.67; N, 3.63%.

Ir10: Yield 91.2 mg (56.4%). ^{1}H NMR (500 MHz, $CDCl_3$) δ 9.05 (d, J = 8.2 Hz, 1H), 8.73 (d, J = 8.2 Hz, 1H), 8.71–8.68 (q, J = 15.3, 8.4 Hz, 2H),8.16–8.07 (dd, J = 15.3, 8.4 Hz, 3H), 7.91 (t, J = 7.2 Hz, 1H), 7.74 (t, J = 7.7 Hz, 1H), 7.60 (q, J = 7.2 Hz, 3H), 7.52 (d, J = 7.9 Hz, 1H), 7.47 (d, J = 7.9 Hz, 1H), 7.41 (dd, J = 8.6, 2.5 Hz, 1H), 7.33 (t, J = 7.7 Hz, 1H), 7.17 (d, J = 8.2 Hz, 1H), 6.84–6.80 (m, 3H), 6.36 (d, J = 7.8 Hz, 1H), 2.68 (s, 3H, CH_3), 1.82 (s, 3H, Cp-CH_3), 1.77–1.75 (m, 6H, Cp-CH_3), 1.66 (s, 3H, Cp-CH_3). ESI-MS (m/z): Calcd for $C_{43}H_{36}N_2ClIr$, 808.2196; Found 773.2501, $[M\text{-}Cl]^+$. Elem. anal. Calcd for $C_{43}H_{36}N_2ClIr$: C, 63.88; H, 4.49; N, 3.47%; Found C, 64.11; H, 4.61; N, 3.38%.

Ir11: Yield 78.4 mg (54.9%). ^{1}H NMR (500 MHz, $CDCl_3$) δ 9.33 (d, J = 8.2 Hz, 1H), 9.08 (dd, J = 10.8, 5.2 Hz, 2H), 8.08 (dd, J = 8.2, 5.3 Hz, 1H), 7.85 (dd, J = 8.5, 5.1 Hz, 2H), 7.66 (d, J = 8.5 Hz, 1H), 7.55 (dd, J = 16.6, 6.6 Hz, 4H), 7.45 (d, J = 8.2 Hz, 1H), 7.31 (d, J = 8.1 Hz, 1H), 6.87 (d, J = 8.8 Hz, 2H), 3.82 (s, 3H, OCH_3), 2.59 (s, 3H, CH_3), 1.76 (s, 15H, Cp-CH_3). ESI-MS (m/z): Calcd for C39H36ON2ClIr, 714.2446; Found 776.2122, $[M\text{-}Cl]^+$. Elem. anal. Calcd for $C_{39}H_{36}ON_2ClIr$: C, 60.33; H, 4.67; N, 3.61%; Found C, 60.56; H, 4.78; N, 3.50%.

Ir12: Yield 93.4 mg (55.7%). ^{1}H NMR (500 MHz, $CDCl_3$) δ 9.30 (d, J = 8.2 Hz, 1H), 8.91 (d, J = 5.1 Hz, 1H), 8.77 (d, J = 5.3 Hz, 1H), 7.93–7.89 (m, 1H), 7.75–7.72 (m, 1H), 7.66 (d, J = 7.9 Hz, 3H),

7.58–7.54 (m, 5H), 7.45 (d, $J = 7.7$ Hz, 2H), 7.33 (d, $J = 8.0$ Hz, 2H), 6.85 (d, $J = 8.8$ Hz, 3H), 3.81 (s, 3H, OCH_3), 2.58 (s, 3H, CH_3), 1.83 (s, 6H, Cp-CH_3), 1.73 (m, 6H, Cp-CH_3). ESI-MS (m/z): Calcd for $C_{44}H_{38}ON_2ClIr$, 838.2302; Found 803.2613, $[M\text{-}Cl]^+$. Elem. anal. Calcd for $C_{44}H_{38}ON_2ClIr$: C, 63.03; H, 4.57; N, 3.34%; Found C, 53.1; H, 3.55; N, 3.37%.

CRediT authorship contribution statement

Ao Lv: Investigation, Writing – original draft. **Guangxiao Li:** Investigation, Writing – original draft. **Pei Zhang:** Investigation. **Rui Tao:** Investigation. **Xiaoshuang Li:** Investigation. **Xueyan Ren:** Investigation. **Peixuan Li:** Investigation. **Xicheng Liu:** Methodology, Investigation, Writing – review & editing. **Xiang-Ai Yuan:** Investigation. **Zhe Liu:** Investigation, Writing – review & editing.

Declaration of competing interest

The authors declare that they have no known competing financial interests or personal relationships that could have appeared to influence the work reported in this paper.

Data availability

Data will be made available on request.

Acknowledgments

We thank the Shandong Provincial Natural Science Foundation (Grant ZR2020MB102 and ZR2022MB047) and the Taishan Scholars Program for their support.

Appendix A. Supplementary data

Supporting Information: Additional experimental details and full characterization data; NMR, MS, crystallographic, UV–Vis and PL spectra; The data of cell cycle, ROS, MMP and apoptosis assay. Supplementary data to this article can be found online at [https://doi.org/10.1016/j.jinorgbio.2024.112612].

References

[1] A. Kastner, T. Mendrina, F. Bachmann, W. Berger, B.K. Keppler, P. Heffeter, C. Kowol, Tumor-targeted dual-action NSAID-platinum(IV) anticancer prodrugs, Inorg. Chem. Front. 10 (2023) 4126–4138.
[2] X. Wang, X. Wang, S. Jin, N. Muhammad, Z. Guo, Stimuli-responsive therapeutic metallodrugs, Chem. Rev. 119 (2019) 1138–1192.
[3] X. Wang, Z. Guo, Targeting and delivery of platinum-based anticancer drugs, Chem. Soc. Rev. 42 (2013) 202–224.
[4] J. Schulz, A.K. Renfrew, I. Císařová, P.J. Dyson, P. Štěpnička, Synthesis and anticancer activity of chalcogenide derivatives and platinum(II) and palladium(II) complexes derived from a polar ferrocene phosphanyl–carboxamide, Appl. Organomet. Chem. 24 (2010) 392–397.
[5] X. He, L. Wei, J. Chen, S. Ge, M. Kandawa-Shultz, G. Shao, Y. Wang, Folate-targeted iridium complexes amplify photodynamic therapy efficacy through ferroptosis, Inorg. Chem. Front. 10 (2023) 4780–4788.
[6] H. Huang, S. Banerjee, P.J. Sadler, Recent advances in the design of targeted iridium(III) photosensitizers for photodynamic therapy, ChemBioChem 19 (2018) 1574–1589.
[7] R. Guan, Y. Chen, L. Zeng, T.W. Rees, C. Jin, J. Huang, Z.S. Chen, L. Ji, H. Chao, Oncosis-inducing cyclometalated iridium(III) complexes, Chem. Sci. 9 (2018) 5183–5190.
[8] N. Roy, U. Sen, S. Chaudhuri, V. Muthukumar, P. Moharana, P. Paira, B. Bose, A. Gauthaman, A. Moorthy, Mitochondria specific highly cytoselective iridium (III)–Cp* dipyridophenazine (dppz) complexes as cancer cell imaging agents, Dalton Trans. 50 (2021) 2268–2283.
[9] P. Moharana, D. Ghosh, P. Paira, Drive to organoruthenium and organoiridium complexes from organoplatinum: next-generation anticancer metallotherapeutics, Inorg. Chem. Commun. 124 (2021) 108364.
[10] Y. Han, G. Jin, Cyclometalated [Cp*M(C^X)] (M = Ir, Rh; X = N, C, O, P) complexes, Chem. Soc. Rev. 43 (2014) 2799–2823.
[11] S. Mukhopadhyay, R. Gupta, R. Paitandi, N. Rana, G. Sharma, B. Koch, L. Rana, M. Hundal, D. Pandey, Synthesis, structure, DNA/protein binding, and anticancer activity of some half-sandwich cyclometalated Rh (III) and Ir (III) complexes, Organometallics 34 (2015) 4491–4506.
[12] J. Ruiz, C. Vicente, C. Haro, D. Bautista, Novel bis-C, N-cyclometalated iridium (III) thiosemicarbazide antitumor complexes: interactions with human serum albumin and DNA, and inhibition of cathepsin B, Inorg. Chem. 52 (2013) 974–982.
[13] Z. Liu, A. Habtemariam, A.M. Pizarro, S.A. Fletcher, A. Kisova, O. Vrana, L. Salassa, P.C.A. Bruijnincx, G.J. Clarkson, V. Brabec, P.J. Sadler, Organometallic half-sandwich iridium anticancer complexes, J. Med. Chem. 54 (2011) 3011–3026.
[14] K. Lo, K. Zhang, Iridium(III) complexes as therapeutic and bioimaging reagents for cellular applications, RSC Adv. 2 (2012) 12069–12083.
[15] S.J. Lucas, R.M. Lord, R.L. Wilson, R.M. Phillips, V. Sridharan, P.C. McGowan, Synthesis of iridium and ruthenium complexes with (N,N), (N,O) and (O,O) coordinating bidentate ligands as potential anti-cancer agents, Dalton Trans. 41 (2012) 13800–13802.
[16] X. Liu, S. Chen, X. Ge, Y. Zhang, Y. Xie, Y. Hao, D. Wu, J. Zhao, X. Yuan, L. Tian, Z. Liu, Dual functions of iridium (III) 2-phenylpyridine complexes: metastasis inhibition and lysosomal damage, J. Inorg. Biochem. 205 (2020) 110983.
[17] X. Zhu, Q. Sun, X. Guo, C. Liang, Y. Zhang, W. Huang, W. Pei, Z. Huang, L. Chen, J. Chen, Cyclometalated ruthenium (II) complexes induced HeLa cell apoptosis through intracellular reductive injury, J. Inorg. Biochem. 247 (2023) 112333.
[18] J. Arshad, M. Hanif, S. Movassaghi, M. Kubanik, A. Waseem, T. Söhnel, S. Jamieson, C. Hartinger, Anticancer Ru (η^6-p-cymene) complexes of 2-pyridine-carbothioamides: a structure–activity relationship study, J. Inorg. Biochem. 177 (2017) 395–401.
[19] C. DuChane, L. Brown, V. Dozier, J. Merola, Synthesis, characterization, and antimicrobial activity of Rh^{III} and Ir^{III} β-Diketonato piano-stool compounds, Organometallics 37 (2018) 530–538.
[20] Z. Liu, P.J. Sadler, Organoiridium complexes: anticancer agents and catalysts, Acc. Chem. Res. 47 (2014) 1174–1185.
[21] W. Wang, Z. Mao, M. Wang, L. Liu, D. Kwong, C. Leung, D. Ma, A long lifetime luminescent iridium (III) complex chemosensor for the selective switch-on detection of Al^{3+} ions, Chem. Commun. 52 (2016) 3611–3614.
[22] C. Jin, J. Liu, Y. Chen, L. Zeng, R. Guan, C. Ouyang, L. Ji, H. Chao, Cyclometalated iridium (III) complexes as two-photon phosphorescent probes for specific mitochondrial dynamics tracking in living cells, Chem. Eur. J. 21 (2015) 12000–12010.
[23] M. Ouyang, L. Zeng, H. Huang, C. Jin, J. Liu, Y. Chen, L. Jia, H. Chao, Fluorinated cyclometalated iridium (III) complexes as mitochondria-targeted theranostic anticancer agents, Dalton Trans. 46 (2017) 6734–6744.
[24] J. Jayabharathi, V. Thanikachalam, M. Perumal, N. Srinivasan, Synthesis, crystal structure, Kamlet-Taft and Catalan solvatochromic analysis of novel imidazole derivatives, J. Fluoresc. 22 (2012) 409–417.
[25] H. No, T. Kim, J. Hong, Iridium (III) complex-based phosphorescent and electrochemiluminescent dual sensor for selective detection of glutathione, Sensors Actuators B Chem. 342 (2021) 129868.
[26] C. Wang, L. Lystrom, H. Yin, M. Hetu, S. Kilina, S. McFarland, W. Sun, Increasing the triplet lifetime and extending the ground-state absorption of biscyclometalated Ir(III) complexes for reverse saturable absorption and photodynamic therapy applications, Dalton Trans. 45 (2016) 16366–16378.
[27] B. Yu, T. Rees, J. Liang, C. Jin, Y. Chen, L. Jia, H. Chao, DNA interaction of ruthenium (II) complexes with imidazo [4, 5-f][1,10] phenanthroline derivatives, Dalton Trans. 48 (2019) 3914–3921.
[28] A. Yoldas, F. Algi, An imidazo-phenanthroline scaffold enables both chromogenic Fe(II) and fluorogenic Zn(II) detection, RSC Adv. 5 (2015) 7868–7873.
[29] Y. Peng, W. He, Q. Niu, C. Tao, X. Zhong, C. Tan, P. Zhao, Mitochondria-targeted cyclometalated rhodium (III) complexes: synthesis, characterization and anticancer research, Dalton Trans. 50 (2021) 9068–9075.
[30] H. Yuan, Z. Han, Y. Chen, F. Qi, H. Fang, Z. Guo, S. Zhang, W. He, Ferroptosis photoinduced by new cyclometalated iridium (III) complexes and its synergism with apoptosis in tumor cell inhibition, Angew. Chem. Int. Ed. 60 (2021) 8174–8181.
[31] G. Gupta, A. Garci, B. Murray, P. Dyson, G. Fabre, P. Trouillas, F. Giannini, J. Furrer, G. Suss-Fink, B. Therrien, Synthesis, molecular structure, computational study and in vitro anticancer activity of dinuclear thiolato-bridged pentamethylcyclopentadienyl Rh(III) and Ir(III) complexes, Dalton Trans. 42 (2013) 15457–15463.
[32] V. Novohradsky, L. Zerzankova, J. Stepankova, A. Kisova, H. Kostrhunova, Z. Liu, P.J. Sadler, J. Kasparkova, V. Brabec, A dual-targeting, apoptosis-inducing organometallic half-sandwich iridium anticancer complex, Metallomics 6 (2014) 1491–1501.
[33] S. Singh, D. Nautiyal, F. Thetiot, N. Poul, T. Goswami, A. Kumar, S. Kumar, Bioinspired Heterobimetallic Photocatalyst (RuIIchrom−FeIIIcat) for Visible-Light-Driven C–H Oxidation of Organic Substrates via Dioxygen Activation, Inorg. Chem. 60 (2021) 16059–16064.
[34] S. Chen, X. Liu, J. Huang, X. Ge, Q. Wang, M. Yao, Y. Shao, T. Liu, X.A. Yuan, L. Tian, Z. Liu, Triphenylamine/carbazole-modified ruthenium (II) Schiff base compounds: synthesis, biological activity and organelle targeting, Dalton Trans. 49 (2020) 8774–8784.
[35] C. Minchew, V. Didenko, Dual detection of nucleolytic and proteolytic markers of lysosomal cell death: DNase II-type breaks and cathepsin D, Methods Mol. Biol. 1554 (2017) 229–236.
[36] R. Khan, I. BinSharfan, S. Alterary, H. Alsaeedi, F. Qais, A. AlFawaz, A. Hadi, A. Alsalme, Organometallic (η^6-p-cymene)ruthenium(II) complexes with thiazolyl-based organic twigs: En route towards targeted delivery via human serum albumin of the potential anticancer agents, Appl. Organomet. Chem. 36 (2022) e6550.

[37] Z. Wang, Z. Lv, X. Liu, Y. Wu, J. Chang, R. Dong, C. Li, X. Yuan, Z. Liu, Anticancer application of ferrocene appended configuration-regulated half-sandwich iridium (III) pyridine complexes, J. Inorg. Biochem. 237 (2022) 112010.
[38] D.K. Soumyashree, D. Reddy, H. Nagarajaiah, L. Naik, H. Savanur, C. Shilpa, M. Kumari, H. Shanavaz, B. Padmashali, Imidazopyridine chalcones as potent anticancer agents: synthesis, single-crystal X-ray, docking, DFT and SAR studies, Arch. Pharm. 356 (2023) e2300106.
[39] C. Liu, X. Liu, X. Ge, Q. Wang, L. Zhang, W. Shang, Y. Zhang, X. Yuan, L. Tian, Z. Liu, J. You, Fluorescent iridium (III) coumarin-salicylaldehyde Schiff base compounds as lysosome-targeted antitumor agents, Dalton Trans. 49 (2020) 5988–5998.
[40] K. Ammann, K. DeCook, P. Tran, V. Merkle, P. Wong, M. Slepian, Collective cell migration of smooth muscle and endothelial cells: impact of injury versus non-injury stimuli, J. Biol. Eng. 9 (2015) 19.
[41] Z. Dean, N. Jamilpour, M. Slepian, P. Wong, Decreasing wound edge stress enhances leader cell formation during collective smooth muscle cell migration, ACS Biomater. Sci. Eng. 5 (2019) 3864–3875.
[42] M. Liu, J. Wang, Q. Qi, B. Huang, A. Chen, X. Li, J. Wang, Nitidine chloride inhibits the malignant behavior of human glioblastoma cells by targeting the PI3K/AKT/mTOR signaling pathway, Oncol. Rep. 36 (2016) 2160–2168.
[43] F. Wang, M. Chen, Y. Lin, H. Zhang, C. Tan, L. Ji, Z. Mao, Dual functions of cyclometalated iridium (III) complexes: anti-metastasis and lysosome-damaged photodynamic therapy, ACS Appl. Mater. Interfaces 9 (2017) 42471–42481.
[44] C. Qian, J. Wang, C. Song, L. Wang, L. Ji, H. Chao, The induction of mitochondria-mediated apoptosis in cancer cells by ruthenium(II) asymmetric complexes, Metallomics 5 (2013) 844–854.
[45] C. Jin, J. Liu, Y. Chen, G. Li, R. Guan, P. Zhang, L. Ji, H. Chao, Cyclometalated iridium(III) complexes with imidazo[4,5-f][1,10]phenanthroline derivatives for mitochondrial imaging in living cells, Dalton Trans. 44 (2015) 7538–7547.
[46] S. Daum, M. Reshetnikov, M. Sisa, T. Dumych, M. Lootsik, R. Bilyy, E. Bila, C. Janko, C. Alexiou, M. Herrmann, L. Sellner, Lysosome-targeting amplifiers of reactive oxygen species as anticancer prodrugs, Angew. Chem. Int. Ed. 56 (2017) 15545–15549.
[47] K. Mahapatra, S. Mishra, B. Behera, S. Patil, D. Gewirtz, S. Bhutia, The lysosome as an imperative regulator of autophagy and cell death, cell Mol, Life Sci. 78 (2021) 7435–7449.
[48] M. He, Q. Yi, W. Zhang, L. Bai, F. Du, Y. Gu, Y. Liu, P. Wei, Evaluation of anticancer activity in vitro and in vivo of iridium(III) polypyridyl complexes, New J. Chem. 43 (2019) 8566–8579.
[49] K. Kaigedal, M. Zhao, I. Svensson, U. Brunk, Sphingosine-induced apoptosis is dependent on lysosomal proteases, Biochem. J. 359 (2001) 335–343.
[50] M. Guicciardi, M. Leist, G. Gores, Lysosomes in cell death, Oncogene 23 (16) (2004) 2881–2890.
[51] C. Pfeffer, A. Singh, Apoptosis: a target for anticancer therapy, Int. J. Mol. Sci. 19 (2018) 448.
[52] J. Li, M. Tian, Z. Tian, S. Zhang, C. Yan, C. Shao, Z. Liu, Half-sandwich iridium (III) and ruthenium (II) complexes containing P^P-chelating ligands: a new class of potent anticancer agents with unusual redox features, Inorg. Chem. 57 (2018) 1705–1716.
[53] W. Wani, U. Baig, S. Shreaz, R. Shiekh, P. Iqbal, E. Jameel, A. Ahmad, S. Mohd-Setapar, M. Mushtaque, L. Hun, Recent advances in iron complexes as potential anticancer agents, New J. Chem. 40 (2016) 1063–1090.
[54] M. Azzopardi, G. Farrugia, R. Balzan, Cell-cycle involvement in autophagy and apoptosis in yeast, Mech. Ageing Dev. 161 (2017) 211–224.
[55] L. Wang, M. Li, P. Cao, C. Zhang, F. Huang, X. Xu, B. Liu, M. Zhang, Astin B, a cyclic pentapeptide from Aster tataricus, induces apoptosis and autophagy in human hepatic L-02 cells, Chem. Biol. Interact. 223 (2014) 1–9.
[56] A. Gatti, A. Habtemariam, I. Romero-Canelon, J. Song, B. Heer, G. Clarkson, D. Rogolino, P.J. Sadler, M. Carcelli, Half-sandwich arene ruthenium (II) and osmium (II) thiosemicarbazone complexes: solution behavior and antiproliferative activity, Organometallics 37 (2018) 891–899.
[57] M. Chen, X. Huang, J. Lai, L. Ma, T. Chen, Substituent-regulated highly X-ray sensitive Os(VI) nitrido complex for low-toxicity radiotherapy, Chin. Chem. Lett. 32 (2021) 158–161.
[58] H. Jiang, Y. Guo, C. Wei, P. Hu, J. Shi, Nanocatalytic innate immunity activation by mitochondrial DNA oxidative damage for tumor-specific therapy, Adv. Mater. 33 (2021) e2008065.
[59] T. Chen, Y. Liu, W. Zheng, J. Liu, Y. Wong, Ruthenium polypyridyl complexes that induce mitochondria-mediated apoptosis in cancer cells, Inorg. Chem. 49 (2010) 6366–6368.
[60] S. Betanzos-Lara, Z. Liu, A. Habtemariam, A. Pizarro, B. Qamar, P.J. Sadler, Organometallic ruthenium and iridium transfer-hydrogenation catalysts using coenzyme NADH as a cofactor, Angew. Chem. Int. Ed. 51 (2012) 3897–3900.
[61] H. Antonicka, K. Choquet, Z. Lin, A. Gingras, C. Kleinman, E. Shoubridge, Organometallic ruthenium and iridium transfer-hydrogenation catalysts using coenzyme NADH as a cofactor, EMBO Rep. 18 (2017) 28–38.
[62] J. Zhang, J. Liu, X. Liu, B. Liu, S. Song, X. He, C. Che, M. Si, G. Yang, Z. Liu, Lysosome-targeted chemotherapeutics: anticancer mechanism of N-heterocyclic carbene iridium (III) complex, J. Inorg. Biochem. 207 (2020) 111063.
[63] L. Dejean, S. Martinez-Caballero, K. Kinnally, Is MAC the knife that cuts cytochrome c from mitochondria during apoptosis? Cell Death Differ. 13 (2006) 1387–1395.
[64] E.C. Stokes, E.E. Langdon-Jones, L.M. Groves, J.A. Platts, P.N. Horton, I.A. Fallis, S. J. Coles, S.J.A. Pope, Cationic, luminescent cyclometalated iridium (III) complexes based on substituted 2-phenylthiazole ligands, Dalton Trans. 44 (2015) 8488–8496.
[65] S.V. Tatarin, P. Kalle, I.V. Taydakov, E.A. Varaksina, V.M. Korshunovc, S. I. Bezzubov, Sterically hindered phenanthroimidazole ligands drive the structural flexibility and facile ligand exchange in cyclometalated iridium (III) complexes, Dalton Trans. 50 (2021) 6889–6900.